2

Microwave Radiometry as a Non-Invasive Temperature Monitoring Modality During Superficial Hyperthermia

Svein Jacobsen
University of Tromsø
Norway

1. Introduction

The application of microwaves in medicine has recently obtained renewed attention within the scientific community through emerging techniques in breast cancer detection (microwave tomography and ultra-wide-band radar imaging), high power ablation as well as microwave angioplasty and lipoplasty (Rosen et al., 2002). Nevertheless, more established techniques reported in the literature based on RF/microwaves are hyperthermia and medical radiometry. During the last decades, a number of research groups have studied various clinical applications based on radio-thermometry for detection of thermal anomalies in subcutaneous, or invasively more deeper, parts of the human body.

The possibility of using microwave radiometry for non-invasive thermometry was originally suggested back in the early 1970's (Edrich & Hardee, 1974; Enander & Larson, 1974) and the sensing principle was denoted *microwave thermography*. Prospected medical applications with highest potential include detection of breast cancer (often in conjunction with infrared thermometry) (Mouty et al., 2000), non-invasive temperature control of superficial (Ohba et al., 1995) and interstitial (Camart et al., 2000) hyperthermia, and control of brain temperatures of newborn infants during mild hypothermia (Hand et al., 2001; Maruyama et al., 2000). Additional applications, which have been investigated, comprise detection of inflammatory arthritis (MacDonald et al., 1994), extravasation rate of drugs (J. Schaeffer & Carr, 1986), changes of blood flow (Gabrielyan et al., 1992) or amount of lung water (Iskander et al., 1984) as well as post-mortem or cerebral temperature monitoring (Al-Alousi et al., 1994).

Microwave radiometry in clinical medicine aims at deriving information on internal body temperature patterns by measurement of natural thermal black-body radiation from tissue in the lower part of the microwave region (<5 GHz). Knowledge on such thermal patterns can give valuable information in clinical disease detection and diagnosis as well as providing quantitative temperature feedback in monitoring of thermal therapeutic processes.

The application of microwave radiometry raises several issues in determination of subcutaneous temperature heterogeneities. Most important is how to optimize design of the receiver hardware by identification of mutual compatible microwave devices with sufficiently low noise figures. The extremely low power levels (-174 dBm/Hz at 37^{o}C body temperature) of electromagnetic thermal noise limit the applicability of microwave radiometers as the usable thermal signal competes both with external electromagnetic interference (EMI) and

the internal noise produced by the hardware. When operated in, or close to, certain communication bands, proper electromagnetic shielding is imperative to stabilize the signal. As for internal noise interference, certain design schemes can be utilized to minimize the overall system noise.

Advances in controllable heating equipment, combined with improvements in non-invasive as well as invasive tissue thermometry techniques (Rhoon & Wust, 2005), have increased the feasibility of using hyperthermia (41-45 ^{o}C for 60 min) as a complementary agent in the treatment of cancer. The effectiveness of hyperthermia treatment is related to the induction of elevated temperatures integrated over time and is often quantified by cumulative equivalent minutes at 43 ^{o}C (CEM43^{o}C). The optimal hyperthermia dose for combinations with radiation or chemotherapy is widely accepted to be 60 min treatment at 43 ^{o}C throughout 90% of measured tumor target temperatures, which represents a CEM43^{o}CT90 thermal dose of 60 min (Sapareto & Dewey, 1984). Temperature homogeneity within the target tissue is an advantage to improve the efficacy of hyperthermia, since a narrow temperature window should bring the response-related minimum tumor temperature closer to the maximum tolerable temperature ($\sim$45 ^{o}C) which avoids undue patient discomfort and complications. Maintaining the targeted temperature distribution within the therapeutic window is a major challenge in hyperthermia in order to attain effective radio- and/or chemosensitization of the treated volume. The therapy goal of obtaining cytotoxic temperatures ($>$42 ^{o}C) for periods of 1 h represents the classical dosimetry view and is supported in studies by Dewhirst *et al.* (1984) and Kapp and Cox (1993). In recent years, however, the biologic rationale for hyperthermia has been subject to discussion (Corry & Dewhirst, 2005). Physiological and cellular effects of mild temperature hyperthermia (39-42 ^{o}C for 1-2 h) are currently under investigation (Calderwood et al., 2005; Dewhirst et al., 2005). The importance of mild temperature hyperthermia related to positive thermo-radiotherapy treatment response is documented in published clinical trials (Jones et al., 2005; Thrall et al., 2005).

In practice, general characterization of tissue temperature distributions with bulk properties like volume average temperature or maximum temperature and location of the maximum can provide very useful realtime feedback information and clinical documentation to an operator. This information is fed back into the heating system for adjustment of antenna power in order to maintain a therapeutic temperature range and avoid side effects from excessive temperatures. Modeling with numerical computations can alternatively or complementary provide additional insight for dose-planning, although unknown patient-specific data (e.g. blood perfusion and power absorption characteristics) limit the reliability of such simulations. Microwave applicators are commonly used for heating of cancerous tissue. Hyperthermia applied to recurrent breast cancer resulted in a complete response rate increase from 31% to 65% in tumors of size smaller than 3 cm (Van der Zee *et al.* 1999). Multi-institutional randomized trials on the same disease all showed similar improvement from adding hyperthermia to radiotherapy (Jones et al., 2005; Vernon et al., 1996). Hyperthermia applicators used in previous efforts have in general been rather bulky and restricted to heating of smaller regions and flat anatomy (Lee, 1995; Stauffer, 2005). However, low cost and expandable printed circuit board (PCB) array construction facilitates development of antennas without the shortcomings of early superficial heating devices. Now lightweight and low profile multi-element array designs have been introduced such as the current sheet applicator (CSA) (Gopal et al., 1992), the contact flexible microstrip applicator (CFMA-12) (Lee et al., 2004), the microstrip spiral applicator (Lee, 1995), the annular aperture and

horseshoe applicators (Carlier et al., 2002), and the Dual Concentric Conductor applicator (DCC) (Rossetto & Stauffer, 2001).

In the field of bio-electromagnetics, thermal considerations are crucial to evaluate dosimetry levels for bio-experiments. A multitude of factors determine the degree of temperature homogeneity in tissue during hyperthermia. This includes heterogeneity in tissue composition which in turn implies local variations in blood flow rate together with thermal and electric conductivity. As a result power absorption, effective heating depth, and efficiency of coupling electromagnetic power into the volume under treatment will vary spatially.

While the vast majority of thermal dosimetry for hyperthermia has been performed using invasive temperature probes to sample a small number of points, there are a number of non-invasive approaches under investigation which can quantify more complete 2-D and 3-D temperature distributions. These techniques include infrared thermography (Tennant & Anderson, 1990), computerized axial tomography (Rutt et al., 1986), ultrasound time-of-flight tomography techniques (Seip & Ebbini, 1995), electrical impedance tomography (Moskowitz et al., 1995), microwave tomography (Chang et al., 1998), magnetic resonance imaging (Samulski et al., 1994), and microwave radiometry (Ohba et al., 1995).

Whereas infrared thermography is able to map thermal emissions from the body surface only, radiometry in the lower microwave region has the potential to detect thermal radiation emitted by subcutaneous tissue up to a depth of several centimeters. Multispectral radiometry has been under investigation as a measurement technique to provide information on temperature depth distributions in tissue. As the radiometric signal strength from a volume element at a particular depth of the medium is correlated with frequency, a multi-frequency scan of a broader band can (at least in principle) be used to map depth temperature gradients. An important limitation of the radiometric observation principle is however the extremely weak signal level of the thermal noise emitted by the lossy material. Consequently, requirements of long integration time (∼5 s) and wide integration bandwidth (∼500 MHz) result in a maximum of 5-6 radiometric bands per antenna within the usable frequency scan range. Even with long data acquisition and signal post-processing times combined with increasingly complex system hardware for multifrequency radiometry, only a few data samples of depth related information are available. For a single antenna system, these sparse data sets can nevertheless produce useful depth-temperature information. Combined with *a priori* information on antenna radiation patterns and tissue dielectric and thermal properties, viable estimates of average temperature in selected tissue volumes can be obtained (Bardati et al., 1991; Camart et al., 2000; Jacobsen & Stauffer, 2003). However, for a full scan of multiple frequencies in a multiple antenna system, the temperature scanning time increases rapidly and can lead to unacceptable cooling during the radiometric listening period while microwave heating power is switched off. Thus from clinical, practical, economical, and technical considerations, the number of radiometric bands should be kept to a minimum (preferably single-band) for temperature monitoring of clinical hyperthermia procedures.

The paper is organized as follows. Section 2 describes the basic radiometric theory (detection scheme, signal model and inversion algorithm) and experimental setup. Section 3 reports experimental phantom results including heating and radiometric antenna layouts, measured antenna return loss as well as radiometric temperature scans of a dynamic heating process. Finally, in Section 4, the findings are evaluated and Section 5 draws conclusions from the research.

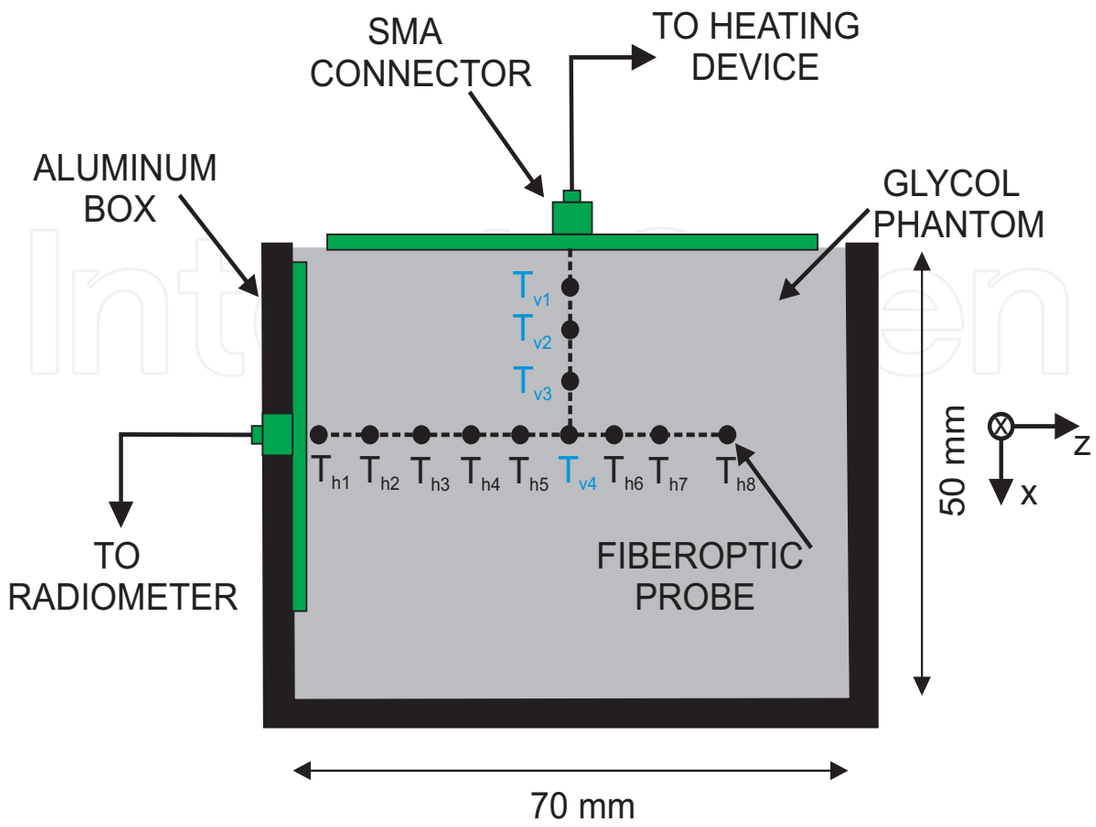

Fig. 1. Pitch-catch mode setup for 915 MHz heating and 3.5 GHz radiometric temperature reading.

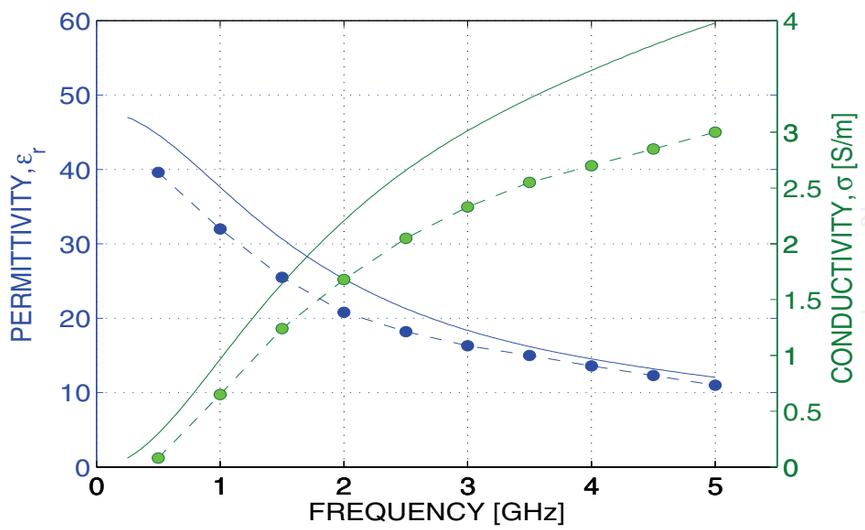

Fig. 2. Dielectric properties of glycol based phantom. Solid line: 90% glycol-10% water mixture. (•): solidified phantom of same mixture.

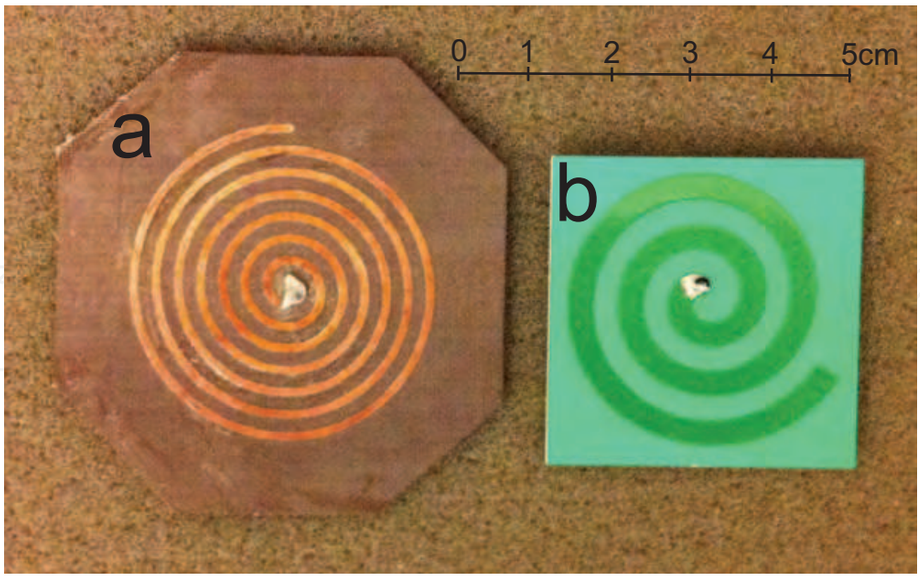

Fig. 3. Antennas used in experiment. a) 915 MHz heating spiral antenna, and b) 3.5 GHz radiometric spiral antenna.

2. Methodology

2.1 Antenna configuration and setup

Fig. 1 depicts the combined heating and temperature measurement configuration considered in the present study. A glycol-water phantom load was solidified with gelatine in a metal box of size $50\times70\times50$ mm^3. We notice from Figure 2, that solidification using gelatine (low permittivity material) lowers both the overall permittivity and conductivity of the applied fluidic phantom. The phantom dielectric properties is similar to that of fat infiltrated mammary tissue.

The five sidewalls of the supporting box, of highly electrically conducting material, provide electromagnetic shielding against competing electromagnetic sources (e.g. cellular phones). However, the aluminum box was not thermally insulated from the surroundings and thus participates in the cooling process as the ambient temperature will influence thermal fluxes within the phantom. Furthermore, the phantom structure was topped with a 50×50 mm^2 spiral heating antenna operated at the medical 915 MHz frequency and driven by a 9 W power source. Arranged in a pitch-catched mode, a smaller 35×35 mm^2 spiral antenna was mounted inside one adjacent sidewall to monitor temperature gradients within the heated volume. The small spiral antenna was connected to a 3.5 GHz single band radiometer with an integration bandwidth of 500 MHz. A photograph of the respective antennas is shown in Figure 3 and measured return loss is depicted in Figure 4. Notice that the small spiral is well matched at the radiometric frequency of 3.5 GHz (S_{11} better than -10 dB) whereas the heating antenna has a return loss of -14 dB at 915 MHz. For correlation with radiometric readings, two perpendicular 1-D temperature profiles (see Figure 1) were established by means of twelve fiberoptic probes rack mounted in a LumiTherm X5R system [1]. The custom made Dicke radiometer used in the experiments has been described in the literature before (Klemetsen et al., 2011). Using miniature surface mount devices (amplifiers, switches and circulators), the front-end printed

[1] www.ipitek.com

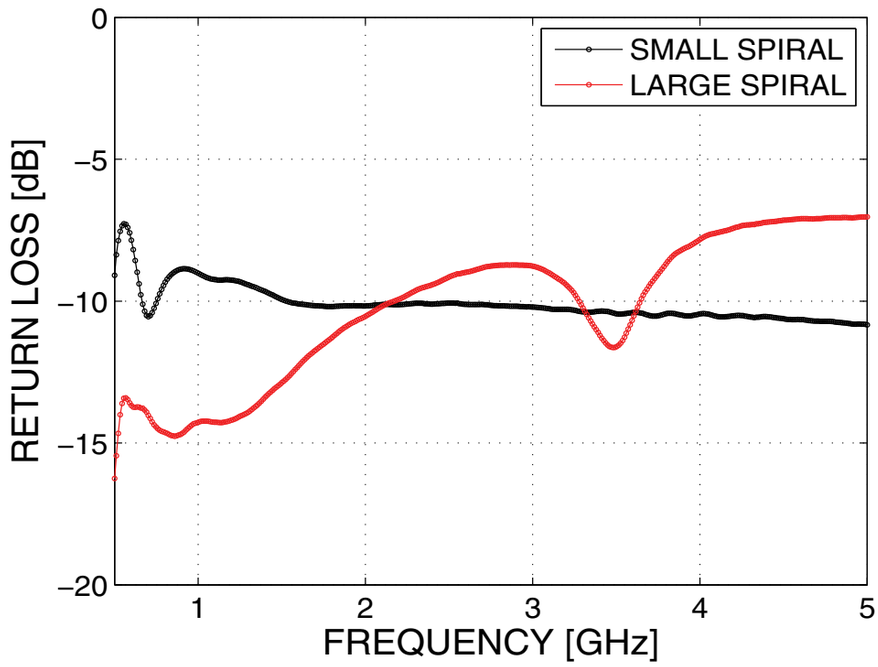

Fig. 4. Measured antenna return loss vs frequency.

circuit board is only 40×50 mm^2 in size. With a detector intergration time of 2 secs and integration bandwidth of 600 MHz, the brightness temperature resolution and theoretical lower accuracy are as low as σ_{T_B}=0.029^{o}C.

2.2 Brightness temperature integral evaluation

Various approaches have been suggested to convert measured radiometric brightness temperatures to an actual temperature distribution within the volume under observation. These methods include parametric (Hand et al., 2001; Ohba et al., 1995) and non-parametric (Bardati et al., 1993; Jacobsen & Stauffer, 2003) modeling. Below we present a 3-D parametric model which leads to a proportionality between the observed and sought parameter.
Consider the general definition of the brightness temperature T_B:

$$T_B = \int_{\Xi} T(\underline{r}) W(f_c, \underline{r}) dV \tag{1}$$

where W is the weighting function (WF) dependent on the spatial variable $\underline{r}$ and center frequency f_c within the integration bandwidth. Ξ is the volume under investigation and dV is an infinitesimal volume element.
The weighting function is normalized according to:

$$\int_{\Xi} W(f_c, \underline{r}) dV \equiv 1 \tag{2}$$

Next, we evaluate the term in Equation (1), which describes the contribution to the lossy load brightness temperature by introducing a parametric model. We assume that both the temperature distribution and weighting function are separable in space with respect to a

Cartesian coordinate system; i.e. $T = T_x(x) \cdot T_y(y) \cdot T_z(z)$ and $W = W_x(x) \cdot W_y(y) \cdot W_z(z)$. Hence, the integral in Equation (1) expands to:

$$T_B = \int_{L_x} T_x(x) W_x(f_c, x)\, dx \int_{L_y} T_y(y) W_y(f_c, y)\, dy \int_{L_z} T_z(z) W_z(f_c, z)\, dz \tag{3}$$

where $L_{x,y,z}$ are the spatial integration lengths within the tissue volume Ξ in x-, y-, and z-direction, respectively. Using the following model functions for the respective factors in Equation (3):

$$T_x = \exp\left(-x/\gamma_{T_x}\right) \tag{4}$$

$$T_y = \exp\left(-y^2/\sigma_{T_y}^2\right) \tag{5}$$

$$T_z = \frac{T_{\max}}{1 + \alpha(z - z_m) + \beta(z - z_m)^2} \tag{6}$$

$$W_x = \frac{1}{\sqrt{\pi}\sigma_{E_x}} \exp\left(-x^2/\sigma_{E_x}^2\right) \tag{7}$$

$$W_y = \frac{1}{\sqrt{\pi}\sigma_{E_y}} \exp\left(-y^2/\sigma_{E_y}^2\right) \tag{8}$$

$$W_z = \frac{1}{d} \exp\left(-z/d\right) \tag{9}$$

where $\sigma_{E_{x,y}}$ are the lateral spatial widths of the weighting function in the x,y-direction, d is the (z-direction) spiral antenna 1/e-sensing depth, γ_{T_x} and σ_{T_y} are the lateral widths of the temperature distribution in the x and y-direction, $T_{\max}$ is the maximum temperature in tissue, and $\{z_m,\alpha,\beta\}$ is a parameter set modeling curvature and asymmetry of the 1-D depth temperature profile. Notice that the required normalization $\int_\Xi W(\underline{r})dV \equiv 1$ is satisfied through the prefixed normalization factors. The 3-D model given in Equations (4)-(9) is a direct generalization of the 1-D model used by Jacobsen and Stauffer (2003) and similar to the 3-D model in Jacobsen and Stauffer (2007).

By carrying out the integration along all directions, and assuming that $L_x = L_y = (-\infty, \infty)$ and $L_z = (0, \infty)$, it is readily shown:

$$T_B = \frac{1}{d\sqrt{1 + \sigma_{E_y}^2/\sigma_{T_y}^2}} \frac{1}{\sqrt{\pi}\sigma_{E_x}^2} \int_{-\infty}^{\infty} \exp(-x/\gamma_{T_x}) \exp(-x^2/\sigma_{E_x}^2)\, dx \cdot \tag{10}$$

$$\int_0^{\infty} \frac{T_{\max}}{1 + \alpha(z - z_m) + \beta(z - z_m)^2} \exp\left(-z/d\right) dz \tag{11}$$

which might be semi-analytically expressed:

$$\begin{aligned} T_B = {} & \frac{T_{\max}}{d} \frac{1}{\sqrt{1 + \sigma_{E_y}^2/\sigma_{T_y}^2}} \frac{1}{\sqrt{\alpha^2 - 4\beta}} \cdot \exp\left(-\frac{\sigma_{E_x}^2}{4\gamma_{T_x}^2}\right) \cdot \\ & \left[\exp\left(\frac{1}{2\beta d}(\alpha - 2\beta z_m - \sqrt{\alpha^2 - 4\beta})\right) E_1\left(\frac{1}{2\beta d}(\alpha - 2\beta z_m - \sqrt{\alpha^2 - 4\beta})\right) - \right. \\ & \left. \exp\left(\frac{\alpha}{2\beta d}(\alpha - 2\beta z_m + \sqrt{\alpha^2 - 4\beta})\right) E_1\left(\frac{1}{2\beta d}(\alpha - 2\beta z_m + \sqrt{\alpha^2 - 4\beta})\right)\right] \end{aligned} \tag{12}$$

$$= \nu(\alpha, \beta, z_m, \gamma_{T_x}, \sigma_{T_y}, \sigma_{E_y}, \sigma_{E_x}, d) T_{\max} \tag{13}$$

Characteristic	Parameter	Nominal value
WF sensing depth	d	6.0 mm
WF lateral width, x-direction	σ_{E_x}	7.0 mm
WF lateral width, y-direction	σ_{E_y}	7.0 mm

Table 1. Parameter values of radiometric antenna.

where $E_1(z) = \int_1^\infty \exp(-zt)t^{-1}dt$ is the exponential integral of first order (Gradshteyn, 1980) which can be tabulated. Here, $\nu \leq 1$ is a proportionality factor that relates the observed and sought parameter.
ν can be derived given that the thermal, dielectric, and geometric parameters are *a priori* known for the setup. From the numerically generated brightness temperature T_B, and using Equation (13), the maximum temperature within the volume can be calculated.
Applying the commercial software package CST Microwave Studio[2], full wave simulation of the radiometric antennas' radiation properties was used to establish the model parameters in Equations (7-9). Numerical values of these runs for the specific phantom are depicted in Table 1.

3. Results

Figure 5 displays the probe-measured temperatures within the phantom as a function of time. We notice in Figure 5(a) the marked dynamic heating bursts displayed by T_{v1} for times less than 2000 secs. The probe closest to the heating antenna reaches a maximum temperature of 40^oC at 1900 secs. Deeper down into the phantom, lower temperatures are observed as intuitively expected. Maximum temperatures at depth are also slightly time-delayed compared to more shallow temperatures due to some minor effects of thermal conduction.
As for the horizontal probes, it is seen in Figures 5 (b) and (c) that the maximum temperature along the z-axis occurs at a depth of 20 mm and 30 mm (27.2^oC). Since probe T_{v4}, located in between T_{h5} and T_{h6}, shows a maximum of 27.4^oC, the z-profile horizontal maximum is located (as anticipated) at the boresight symmetry line of the heating antenna.
To get an overview of the dynamic heating process taking place within the phantom, perpendicular to and in the observation direction of the radiometric antenna, temperature profiles along the z- and x-axis are plotted in Figure 6 at selected points in time. The shape of the profiles in both directions is modeled accurately by Equations (4) and (6). Notice the smooth shape of the model function in the z-direction with a maximum plateau underneath the center of the heating antenna. In addition, the x-direction temperature gradient is significant (up to $1^oC/mm$), especially subsequent to the heating sequences taking place for times less than 1800 secs. During the cooling process, the decay curves flatten and eventually become spatially constant.
Table 2 quantifies the parameter values obtained for the snapshots in Fig 6. Observe the relatively small values of γ_{T_x} in the heating phase. During the cooling process (time$\geq$2150 secs), large values of γ_{T_x} model the x-direction temperature profile, meaning that it is virtually flat (homogeneous temperature) lateral to the radiometric observation axis.
Based on Table 1 and Equations (4)-(9), the brightness temperature T_B can be estimated through Equation (12) for the dynamic run discussed above.

[2] www.cst.com

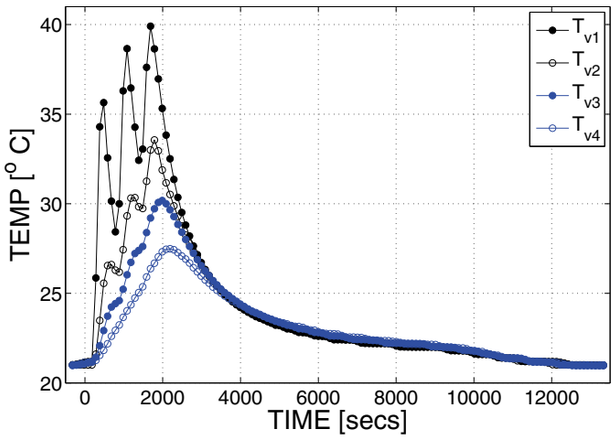

(a) Vertical probes in Fig. 1

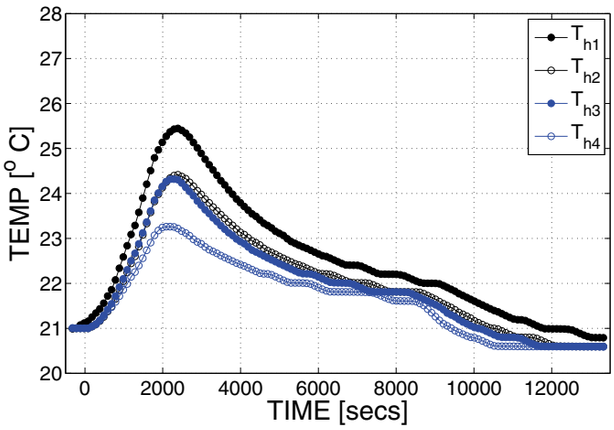

(b) Horizontal probes (first 4) in Fig. 1

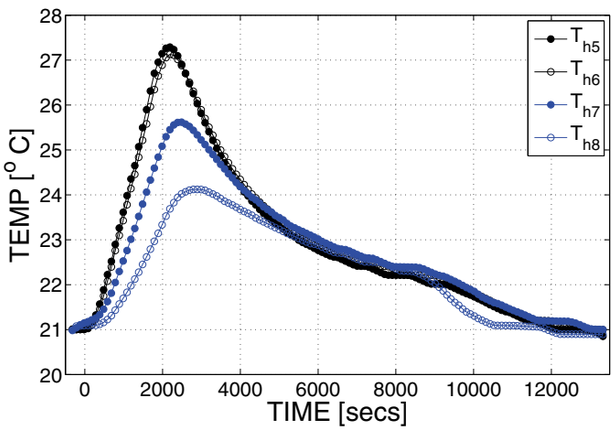

(c) Horizontal probes (last 4) in Fig. 1

Fig. 5. Fiberoptic probe temperature measurements vs time.

To evaluate the validity of the radiometric model, comparisons are made with the measured temperatures derived from the miniature radiometer. Figure 7 (upper panel) shows this comparison for two different models. This includes a simplified 1-D parametric model where variations along the transversal axis (x-direction) are neglected. In this case it is implicitly assumed that $\gamma_{T_x} = \infty$. In the other 2-D model, also temperature variations in the transverse direction are adopted into the model.
From the deviation plot in Figure 7 (lower panel) we notice improved performance (smaller deviation between measurement and model) in the heating phase (times less than 2000 secs) when the more advanced 2-D model is applied. A quantitative analysis of the respective models shows an improvement in the standard deviation of the instantaneous error from $\sigma_{T_{1-D}}$=0.28^{o}C in the 1-D case to $\sigma_{T_{2-D}}$=0.21^{o}C in the 2-D case.
During the cooling phase, $\gamma_{T_x} \gg 1$ and the difference in performance between the 1-D and 2-D model should be negligible. This is verified in Figure 7 (lower panel) as only marginal deviations in performance are observed for times greater than 3000 secs.
One pertinent question is to what extent the maximum temperature within the heated volume can be predicted given a measured brightness temperature; information that can be valuable to a system operator. The numerical span of the model parameters in Table 2 indicates that there exists no unique parameter combination that provides an overall proportionality factor ν in Equation (13). However, as seen in Figure 8, a constant ν still provides correlated estimates between radiometrically estimated and probe measured maximum temperatures within the heated volume.

4. Discussion

Hyperthermia has been demonstrated to be an efficacious adjuvant to other conventional approaches for cancer therapy. Breast cancer is one of the most prevalent forms of cancer in women and local control of this disease remains an issue of continually increasing magnitude. Due to uncertainties associated with the actual electromagnetic power deposition and thus the resulting temperature distribution in an arbitrary, heterogeneous, and temporally varying tissue configuration, some type of temperature feedback control is essential for safe and reliable heating performance of any hyperthermic system. With its non-invasive character and being a totally passive sensing principle, microwave radiometry has the potential to allow thermometry of subcutaneous tissues to a depth of some centimeters. As opposed to IR radiometry, microwave radiometry does not provide high-resolution thermographic mapping of the tissue, since lateral spatial resolution is limited by antenna size and spacing, which are

Time [s]	$\alpha[mm^{-1}]$	$\beta[mm^{-2}]$	$z_m[mm]$	$\gamma_{T_x}[mm]$
500	0.0192	0.00519	23.1	5.1
750	-0.0355	0.00538	19.7	11.2
1170	-0.0422	0.00411	18.3	9.8
1650	0.0632	0.00215	38.1	11.1
2150	-0.0571	0.00118	0.65	27.1
3100	-0.0355	0.00183	17.6	154.0
3642	-0.0141	0.00155	24.3	∞
6135	-0.0154	0.00092	27.3	∞
9700	-0.0290	0.00468	26.1	∞

Table 2. Numerical parameter values of temperature profiles in Figure 6.

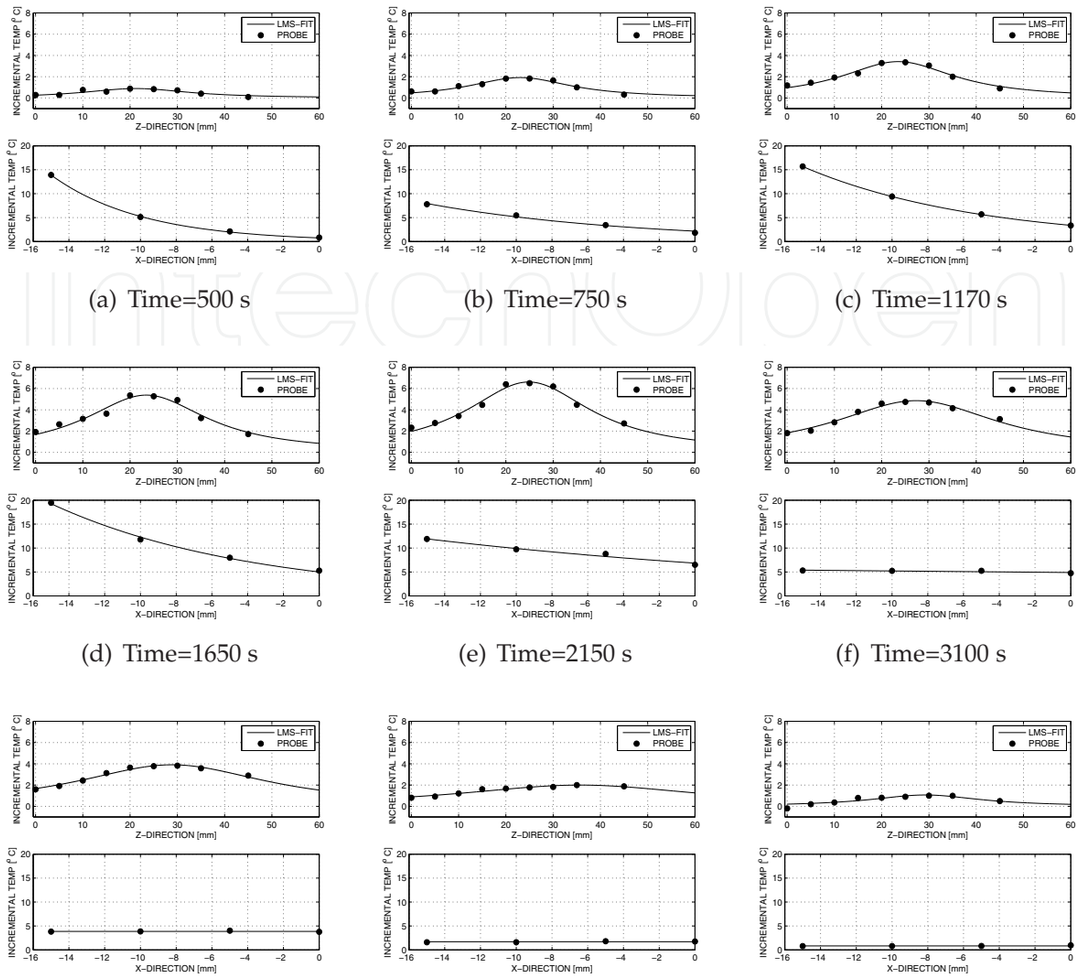

(a) Time=500 s (b) Time=750 s (c) Time=1170 s

(d) Time=1650 s (e) Time=2150 s (f) Time=3100 s

(g) Time=3642 s (h) Time=6135 s (i) Time=9700 s

Fig. 6. Fiberoptic temperature profiles in phantom along two orthogonal axes for different times. Solid line: Fitted model in Equations (4) and (6).

in the order of centimeters. This limitation, combined with the necessity of proper shielding to avoid interfering signals from other competing EM sources, put constraints on the realization of this observation technique.

Since medical microwave radiometry only offers sparse temperature data sets, either *a priori* experimental knowledge (Mizushina et al., 1993) or complementary thermal modeling (Bardati et al., 1993) have been proposed to help solve the underdetermined inverse problem of characterizing temperature distributions at depth in living tissue.

In the present study we evaluate the robustness of a proposed temperature estimator scheme based on single-band radiometric scanning. A bistatic antenna pitch-catch setup on a glycol based phantom was used to test the performance of a single-band miniature microwave radiometer. One large spiral antenna was used to heat the volume under investigation using the medical 915 MHz frequency. A similar, but smaller, spiral antenna was also put flush to the phantom to observe thermal radiation. Since no blood perfusion is present in the phantom, only 9 W was required to heat the volume up to therapeutic hyperthermia temperatures

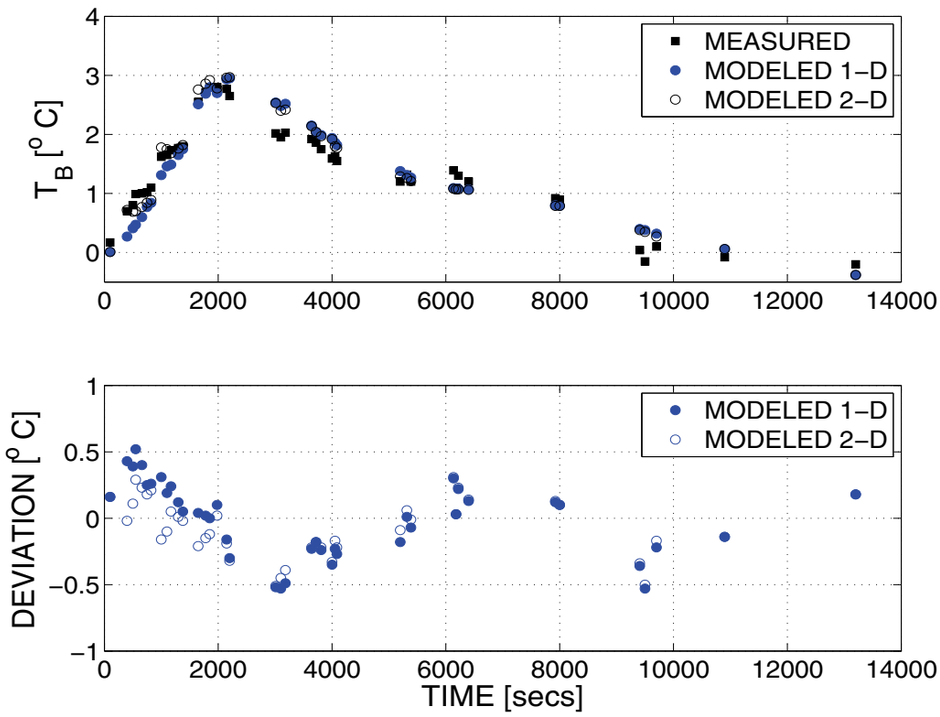

Fig. 7. Differential radiometric brightness temperature versus time. Measured and 1-D & 2-D models (upper panel), deviation between models and measurements (lower panel).

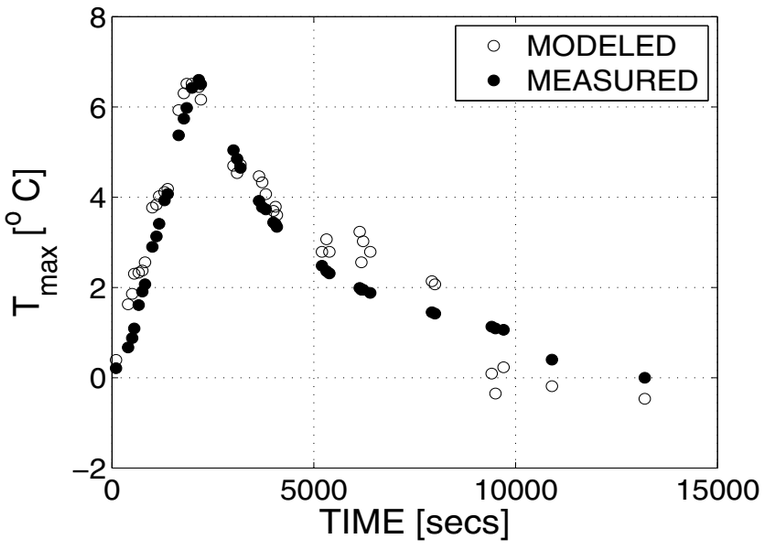

Fig. 8. Measured and radiometrically modeled (ν=0.65 in Equation (13)) maximum temperature within heated phantom vs time.

(>40^{o}C). The heating was conducted in several burst to mimic the clinical scenario of interspersed heating and radiometric temperature reading. In order to investigate long term

stability of the radiometric instrumentation, temperature readings were also performed in the cooling phase, in which the phantom interchanged energy with the surroundings (ambient temperature of 21^oC) back to the initial pre-heating state.
Overall, the concordance between the modeled and measured brightness temperatures was satisfactory, with deviations typically less than $\pm 0.3^oC$ of the maximum T_B temperature elevation of 3.0^oC. Since the proportionality factor $\nu < 1$ in Equation (13) , the maximum temperature elevation in the phantom is somewhat higher than the maximum observed brightness temperature. According to Figure 8, the maximum increase along the radiometric observation axis is about 6.5^oC occuring at z=25 mm (see Figure 6) 2150 secs into the experiment.
The pitch-catch experimental setup produces temperature gradients in two directions. Hence, the radiometric weighting function is generally 2-D in cases where temperature equilibrium is not obtained along the transversal x-axis. Thus, one pertinent question is whether the proposed 2-D model performs better than the simplified 1-D model in such cases. This is indeed the case as can be observed in the heating phase of the experiment (Figure 7) displaying an improvement of typically 0.2^oC in accuracy. However, when the transversal temperature gradient can be neglected, the 1-D and 2-D models perform equally well.
Finally, the ability to predict the maximum temperature within the heated volume given a single-band radiometric reading was investigated. In the heating phase, a high degree of concordance was observed between measured and estimated maximum temperature. As the cooling process started, larger deviations were observed as a consequence of more extreme values of the model parameters (see Figure 8). Fortunately, the cooling phase is less realistic with respect to a clinical hyperthermia scenario, as more steady state conditions with temperatures above 40^oC are expected in such cases.

5. Conclusion

The accuracy of using mono-frequency microwave radiometry to retrieve maximum bulk temperatures of a heated glycol-based phantom was experimentally studied using a miniature radiometer operating at 3.5 GHz. A computationally fast retrieval scheme, based on a single brightness temperature, was implemented to predict the dynamic brightness temperature during both the heating and cooling part of the experiment. In cases of highest degree of temperature inhomogeneity within the phantom, more advanced temperature distribution models were needed to predict the observed variations. As the temperature distribution became more homogeneous towards the end of the experiment, 1-D temperature profiles were sufficient to adequately model the observations.

6. References

Al-Alousi, L. M., Anderson, R. A. & Land, D. V. (1994). A non invasive method for postmortem temperature measurement using a microwave probe, *Forensic Science Int.* 64: 35–46.

Bardati, F., Brown, V. J. & Bernardo, G. D. (1991). Multi-Frequency Microwave Radiometry for Retrieval of Temperature Distributions in the Human Neck, *The Journal of Photographic Science* 39: 157–160.

Bardati, F., Brown, V. J. & Tognolatti, P. (1993). Temperature Reconstruction in a Dielectric Cylinder by Multi-Frequency Microwave Radiometry, *Journal Electromagnetic Waves and Applications* 7(1): 1549–1571.

Calderwood, S. K., Theriault, J. R. & Gong, J. (2005). How is the immune response affected by hyperthermia and heat shock proteins?, *International Journal Hyperthermia* 21: 713–716.

Camart, J. C., Despretz, D., Prevost, B., Sozanski, J. P., Chivé, M., & Pribetich, J. (2000). New 434 MHz interstitial hyperthermia system monitored by microwave radiometry: theoretical and experimental results, *Int Journal of Hyperthermia* 16: 95–111.

Carlier, J., Camart, J. C., Dubois, L. & Priebetich, J. (2002). Modeling of planar applicators for microwave thermotherapy, *IEEE Transactions Microwave Theory Techniques* 50(12): 3036–3042.

Chang, J. T., Paulsen, K., Meaney, P. & Fanning, M. (1998). Non-invasive thermal assessment of tissue phantoms using an active near field microwave imaging technique, *International Journal Hyperthermia* 14(6): 513–534.

Corry, P. & Dewhirst, M. (2005). Special Issue: Thermal Medicine, Heat Shock Proteins and Cancer, *International Jornal of Hyperthermia* 8: 675–790.

der Zee, J. V., Holt, B. V. D., Rietveld, P. J. M. & et al. (1999). Reirradiation combined with hyperthermia in recurrent breast cancer results in worthwhile local palliation, *British Journal Cancer* 99: 483–490.

Dewhirst, M., Sapareto, S. & Connor, W. G. (1984). Importance of minimum tumor temperature in determining early and long term responses of spontaneous canine and feline tumors to heat and radiation, *Cancer Research* 44: 43–50.

Dewhirst, M. W., Vujaskovic, Z., Jones, E. & Thrall, D. (2005). *International Journal of Hyperthermia* 8: 779–790.

Edrich, J. & Hardee, P. C. (1974). Thermography at millimeter wavelength, *Proceedings of IEEE* 62: 1391–1392.

Enander, B. & Larson, G. (1974). Microwave radiometric measurements of the temperature inside a body, *Electronic Letters* 10: 317–318.

Gabrielyan, E. S., Khachatryan, L. A., Nalbaudyan, S. G., & Gregorian, F. A. (1992). Microwave method for determining cerebral blood flow", *Methods (New York: Plenum)* pp. 713–715.

Gopal, M. K., Hand, J. W., Lumiori, M. L. D., Alkhairi, S., Paulsen, K. D. & Cetas, T. C. (1992). Current sheet applicator arrays for superficial hyperthermia of chestwall lesions, *International Journal of Hyperthermia* 8(2): 227–240.

Gradshteyn (1980). *Table of Integrals, Series, and Products*, Academic Press, San Diego.

Hand, J. W., Leeuwen, G. M. J. V., Mizushina, S., de Kamer, J. B. V., Maruyama, K., Sugiura, T., Azzopardi, D. V., & Edwards, A. D. (2001). Monitoring of Deep Brain Temperature in Infants Using Multi-Frequency Microwave Radiometry and Thermal Modeling, *Physics in Medicine and Biology* 46: 1885–1903.

Iskander, M. F., Durney, C. H., Grange, T., & Smith, C. S. (1984). Radiometric Technique for Measuring Changes in Lung Water, *IEEE Trans. Microwave Theory Techiques* MTT-32: 554–556.

J. Schaeffer, A. El Mahdi, A. H. & Carr, K. (1986). Detection of extravasation of antineoplastic drugs by microwave radiometry, *Cancer Letters* 31: 285–291.

Jacobsen, S. & Stauffer, P. (2003). Nonparametric 1-D Temperature Restorartion in Lossy Media Using Tikhonov Regularization on Sparse Radiometry Data, *IEEE Transactions Biomedical Engineering* 50(2): 178–188.

Jacobsen, S. & Stauffer, P. R. (2007). Can we settle with single-band radiometric temperature monitoring during hyperthermia teatment of chestwall recurrence of

breast cancer using a dual-mode transceiving applicator, *Physics in Medicine and Biology* 52(4): 911–928.

Jones, E. L., Oleson, J. R., Prosnitz, L., Samulski, T., Vujaskovic1, Z., Yu, D., Sanders, L. & Dewhirst, M. (2005). Randomized trial of hyperthermia and radiation for superficial tumors, *Journal of Clinical Oncology* 23: 3079–3085.

Kapp, D. S. & Cox, R. S. (1993). Cumulative minutes of isoeffective hyperthermia with T90=43^{o}C is the treatment parameter most predictive for outcome in patients with metastatic adenocarcinoma of the breast and single tumor nodules per treatment field, *International Journal of Radiation Oncology Biology Physics* 27: 315.

Klemetsen, O., Birkelund, Y., Jacobsen, S. K., Maccarini, P. & Stauffer, P. R. (2011). Design of Medical Radiometer Front-End for Improved Performance, *Progress In Electromagnetic Research B* 27: 289–306.

Lee, E. R. (1995). Electromagnetic superficial heating technology, *in* P. Fessenden & C. C. Vernon (eds), *Thermoradiotherapy and Thermochemotherapy*, Springer-Verlag, pp. 193–217.

Lee, W. M., Gelvich, E. A., der Baan, P. V., Mazokhin, V. N. & Rhoon, G. C. V. (2004). Assessment of the performance characteristics of a prototype 12-element capacitive contact flexible microstrip applicator (CFMA-12) for superficial hyperthermia, *International Journal of Hyperthermia* 20(6): 607–624.

MacDonald, A. G., Land, D. V. & Sturrock, R. D. (1994). Microwave thermography as a non-invasive assessment of disease activity in inflammatory arthritis, *Clinical Rheumatology* 13: 589–592.

Maruyama, K., Mizushina, S., Sugiura, T., van Leeuwen, G. M. J., Hand, J. W., Marrocco, G., Bardati, F., Edwards, A., Azzopradi, D. & Land, D. (2000). Feasibility of Noninvasive Measurement of Deep Brain Temperature in Newborn Infants by Multifrequency Microwave Radiometry, *IEEE Trans Microwave Theory Techniques* 48: 2141–2147.

Mizushina, S., Shimizu, T., Suzuki, K., Kinomura, M., Ohba, H. & Sugiura, T. (1993). Retrieval of Temperature-Depth Profiles in Biological Objects from Multi-Frequency Microwave Radiometric Data, *Journal Electromagnetic Waves and Applications* 7(11): 1515–1547.

Moskowitz, M. J., Ryan, T. P., Paulsen, K. D. & Mitchell, S. E. (1995). Clinical implementation of electrical-impedance tomography with hyperthermia, *International Journal Hyperthermia* 11(2): 141–149.

Mouty, S., Bocquet, B., Ringot, R., Rocourt, N. & Devos, P. (2000). Microwave radiometric imaging (MWI) for the characterization of breast tumors, *The European Journal of Applied Physics* AP 10: 73–78.

Ohba, H., Kinomura, M., Ito, M., Sugiura, T. & Mizushina, S. (1995). Multi-frequency microwave radiometry for noninvasive thermometry using a new temperature profile model function, *Trans. IEICE Electron.* E-78: 1071–1081.

Rhoon, G. C. V. & Wust, P. (2005). Special Issue: Non Invasive thermometry for thermotherapy, *International Journal of Hyperthermia* 21(6): 489–600.

Rosen, A., Stuchly, M. A. & Vorst, A. V. (2002). Applications of RF/Microwaves in Medicine, *IEEE Trans. Microwave Theory Techniques* 50: 963–974.

Rossetto, F. & Stauffer, P. R. (2001). Theoretical characterization of dual concentric conductor microwave applicators for hyperthermia at 433 MHz, *International Journal Hyperthermia* 17(3): 258–270.

Rutt, B. K., Fike, J. R. & Stauffer, P. R. (1986). *In: 34th Meeting of Radiation Research Society; 1986; Las Vegas* p. 35.

Samulski, T. V., Clegg, S. T., Das, S., Macfall, J. & Prescott, D. M. (1994). Application of a new techology in clinical hyperthermia, *International Journal Hyperthermia* 10(3): 389–394.

Sapareto, S. A. & Dewey, W. C. (1984). Thermal dose determination in cancer therapy, *International Journal of radiation Oncology, Biology & Physics* 10: 787–800.

Seip, R. & Ebbini, E. S. (1995). Noninvasive Estimation of Tissue Temperature Response to Heating Fields Using Diagnostic Ultrasound, *IEEE Transactions on Biomedical Engineering* 42(8): 828–839.

Stauffer, P. (2005). Evolving technology for thermal therapy of cancer, *Internation Journal of Hyperthermia* 21(8): 731–744.

Tennant, A. & Anderson, A. P. (1990). A robot-controlled microwave antenna system for uniform hyperthermia treatment of superficial tumours with arbitrary shape, *International Journal of Hyeprthermia* 6(1): 193–202.

Thrall, D. E., LaRue, S. M., Yu, D., Samulski, T., Sanders, L., Case, B., Rosner, G., Azuma, C., Poulsen, J., Pruitt, A. F., Stanley, W., Hauck, M. L., Williams, L., Hess, P. & Dewhirst, M. (2005). Thermal dose is related to duration of local control in canine sarcomas treated with thermoradiotherapy, *Clinical Cancer Research* 11: 5206–5214.

Vernon, C. C., Hand, J. W., Field, S. B., Machin, D., Whaley, J. B., van der Zee, J., van Putten, W. L. J., van Rhoon, G. C., van Dijk, J. D. P., Gonzalez-Gonzalez, D., Liu, F. F., Goodman, P. & Sherar, M. (1996). Radiotherapy with or without hyperthermia in the treatment of superficial localized breast cancer: Results from five randomized controlled trials, *International Journal Radiation Oncology Biology Physics* 35(4): 731–744.

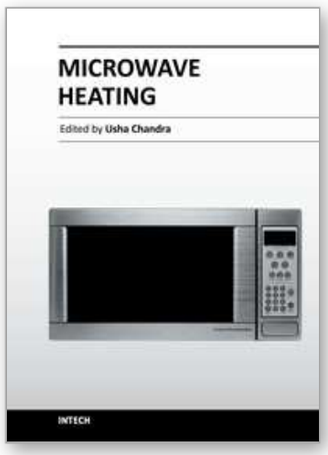

Microwave Heating

Edited by Dr. Usha Chandra

ISBN 978-953-307-573-0
Hard cover, 370 pages
Publisher InTech
Published online 27, July, 2011
Published in print edition July, 2011

The Microwave heating has not only revolutionized the food industry but also has extended its wings widely towards its multidimensional applications. Thus it has opened new vistas of potential research in science and technology. The book is compiled into Seventeen Chapters highlighting different aspects varying from epistemological discussion to applicability of conceptual constructs. The inclusion of discussion on the avenues in the field of Chemistry, Health & Environment, Medical Sciences and Technology makes it an exquisite work for the aspirant Researchers. As the text book for the beginners, it is designed fundamentally to be a reference monograph to the experts providing a passage for future research. The plethora of literatures are available on Microwave Applications but they seldom direct their readers to concentrate on the key aspects behind the success in microwave applications in different fields. Here is the attempt to fill up the gap with this book.

INTECH
open science | open minds

InTech Europe
University Campus STeP Ri
Slavka Krautzeka 83/A
51000 Rijeka, Croatia
Phone: +385 (51) 770 447
Fax: +385 (51) 686 166
www.intechopen.com

InTech China
Unit 405, Office Block, Hotel Equatorial Shanghai
No.65, Yan An Road (West), Shanghai, 200040, China
中国上海市延安西路65号上海国际贵都大饭店办公楼405单元
Phone: +86-21-62489820
Fax: +86-21-62489821

IntechOpen